Theoretical study of InGaAsP-InP active microring

Yunhong Ding, Xiaobei Zhang, Xinliang Zhang, Dexiu Huang*

Wuhan National Laboratory for Optoelectronics, School of Optoelectronics Science and Engineering,

Huazhong University of Science and Technology, Wuhan, 430074, Hubei, People's Republic of China

hustdyh@smail.hust.edu.cn, *wnlo2@mail.hust.edu.cn

ABSTRACT

The electrically pumped InGaAsP/InP active microring has been theoretically analyzed and numerically simulated based on subsection model, with carrier rate equation and amplified spontaneous emission taken into account. After the subsection model is introduced in detail, the spectrum characteristics are numerically investigated. The simulation results show that spectrum characteristics will shift under different pump current and injected light power. The performances of an optical on/off switching utilizing pump-probe method based on InGaAsP/InP active microring are investigated. The results show that if we choose probe light off resonation initially, and pump light on resonation, only several hundred of microwatt power of pump light can realize the probe light on/off conversion. Such a potential will be applied in many other optical applications with ultra low power consumption. However, carrier lifetime will be the main factor restricting the characteristics of electrically pumped active microring due to the fact that the refractive index change is induced by carrier density change.

Key words: Electrically injected; Active microring; Subsection; Pump-probe method; Optical Switching

1. INTRODUCTION

Active microring is an attractive optical element for its functionality, and it has received considerable attention in many optical applications, such as active microring lasers[1], bistable element[2, 3], flip-flop memory unit[4] and so on. The main method analyzing microring is Finite-Difference Time-Domain method[5], which is a time-consumption solution, and if we use it in dynamic simulation of active micriring, the computation will be more massive for the reason that

Photonics and Optoelectronics Meetings (POEM) 2008: Optoelectronic Devices and Integration
edited by Liming Zhang, Michael J. O'Mahony, Proc. of SPIE Vol. 7279, 72790N · © 2009 SPIE
CCC code: 0277-786X/09/$18 · doi: 10.1117/12.821168

carrier rate equation must be taken into account. Subsection model has been successfully applied in the dynamical characteristics analysis of semiconductor optical amplifier (SOA)[6], including cross-gain-modulation, cross- and self-phase-modulation[7] and super fast phenomenon[8]. Considering the same gain medium of □-□ material system based active microring as the semiconductor optical amplifier, the subsection model can be also utilized to describe the active microring.

In this paper, we theoretically analyzed and numerically simulated the electrically pumped InGaAsP/InP active microring based on subsection model, associating with carrier rate equation. After the subsection model is introduced in detail, the spectrum characteristics are numerically simulated. After that, the performances of an optical switching utilizing pump-probe method based on InGaAsP/InP active microring are investigated. The results show that if we choose pump light on resonation, and probe light off resonation initially, only several hundred of microwatt power of pump light can realize the probe light on/off conversion. Such a potential will be applied in many other optical applications with ultra low power consumption. However, carrier lifetime will be the main factor restricting the characteristics of electrically pumped active microring.

2. THEORETICAL MODEL

The analytical model of the □-□ active microring is shown in Fig. 1. The active microring is analyzed by two individual sections: waveguide and coupler. The waveguide section is divided into several subsections. In each subsection, the light field satisfies the propagation equation with amplified spontaneous emission (ASE) taken into account. Meanwhile, each junction of the subsection is assumed to be lossless and without reflection. In the coupling area, the light field is described by the coupling matrix.

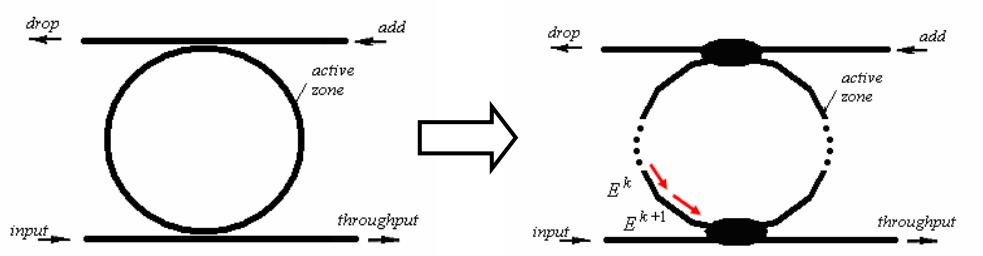

Fig. 1. Analytical model of active microring

The light propagating in each subsection is described by the full-wave model as follows, since only the full wave model can always handle the interaction between the signal and the spontaneous emission in an incoherent manner, which gives the closest description of what happened in each subsection in reality[9].

$$\frac{1}{v_g}\frac{\partial E_{(CW,CCW)}(z,t,\lambda_k)}{\partial t}\pm\frac{\partial E_{(CW,CCW)}(z,t,)}{\partial z}$$
$$=\left\{-j\left(\beta(\lambda_k)+\frac{1}{2}\Gamma\alpha_m g(z,t,\lambda_k)\right)+\frac{1}{2}\left(\Gamma g(z,t,\lambda_k)-\alpha_s\right)\right\}\times E_{(CW,CCW)}(z,t,\lambda_k)+s_{(CW,CCW)}(z,t,\lambda_k) \quad (1)$$

Where $E_{(CW,CCW)}$ ($m^{-3/2}$) are the clockwise and counter-clockwise traveling optical light waves respectively, v_g (m/s) denotes the group velocity, λ_k is the wavelength in the spontaneous emission section subsection, $\beta(\lambda_k)$ (m^{-1}) is the wave propagation constant , Γ is the confinement factor, α_m is the linewidth enhancement factor, g (m^{-1}) is the material gain and α_s (m^{-1}) is the modal loss. The ASE noise contribution can be evaluated by a Gaussian-distributed random number generator with a self-correlation function as follows[10]:

$$\left\langle s_{(CW,CCW)}(z,t,\lambda_k)\, s^*_{(CW,CCW)}(z,t,\lambda_k)\right\rangle = \gamma \frac{R_{sp}(z,t,\lambda_k)}{dz v_g}\delta(z-z')\delta(t-t')\delta(\lambda_k-\lambda_{k'}) \tag{2}$$

Where γ is spontaneous coupling coefficient, R_{sp} ($s^{-1}m^{-3}$) is the spontaneous emission rate, and *dz* is the length of each subsection introduced by the spatial discretization of the active zone. The material gain g and spontaneous emission rate R_{sp} can be evaluated by the two energy band model[6]:

$$g_m(\omega_0) = \frac{c^2}{2n_1^2\omega_0^2\tau}\left(\frac{2m_e m_{hh}}{\hbar(m_e+m_{hh})}\right)^{3/2} \times \left(\omega_0 - \frac{E_g}{\hbar}\right)^{1/2}\left(f_c(\omega_0) - f_v(\omega_0)\right) \tag{3}$$

$$R_{sp}(\omega_k) = \frac{dv}{\pi\tau}\left(\frac{2m_e m_{hh}}{\hbar(m_e+m_{hh})}\right)^{3/2} \times \left(\omega_k - \frac{E_g}{\hbar}\right)^{1/2} f_c(\omega_k)\left(1-f_v(\omega_k)\right) \tag{4}$$

Where *c* is velocity of propagation of light in vacuum, n_1 is active region refractive index, ω_0 is the angular frequency of the injected light, τ is the radiative carrier recombination lifetime, $\hbar$ is the normalized Planck's constant, m_e and m_{hh} are the effective mass of an electron in conduction band and an heavy hold in valence band respectively. $f_c(\omega_0)$ and $f_v(\omega_0)$ are the Fermi-Dirac distributions which determine the occupation probabilities for the electrons in the conduction band and the valence band respectively. E_g is the bandgap energy. For the fact that the injected light into the active microring is a pulse with several hundred ps or a CW light in this paper, the super fast effect is negligible.

The carrier rate equation is described by

$$\frac{dN(z,t)}{dt} = \frac{I}{eV} - \left[A + BN(z,t) + CN^2(z,t)\right]N(z,t) - \sum_{k=1}^{N_d}\Gamma v_g g(z,t,\lambda_k)\left|E_{CW}(z,t,\lambda_k) + E_{CCW}(z,t,\lambda_k)\right|^2 \tag{5}$$

In the coupling area as shown in Fig. 2, the light field satisfies the transfer matrix as follows

$$\begin{bmatrix} E_o \\ E^1 \end{bmatrix} = \begin{bmatrix} r & -j\kappa \\ -j\kappa & r \end{bmatrix}\begin{bmatrix} E_i \\ E^N \end{bmatrix} \tag{6}$$

Where r and κ denotes the coupling and transparent coefficient respectively. Regardless of the coupling loss in

the coupling region, r and κ satisfy $\kappa^2 + r^2 = 1$.

3. SIMULATION RESULTS

3.1 Spectrum calculation

To calculate the spectrum characteristics, a steady-state numerical algorithm is required. The flowchart of the algorithm is shown in Fig. 3. The input light is injected from the counter-clockwise direction, to simplify the computation and considering the ASE noise is relatively low compared to the signal power, only the noises propagating along counter-clockwise direction are taken into account.

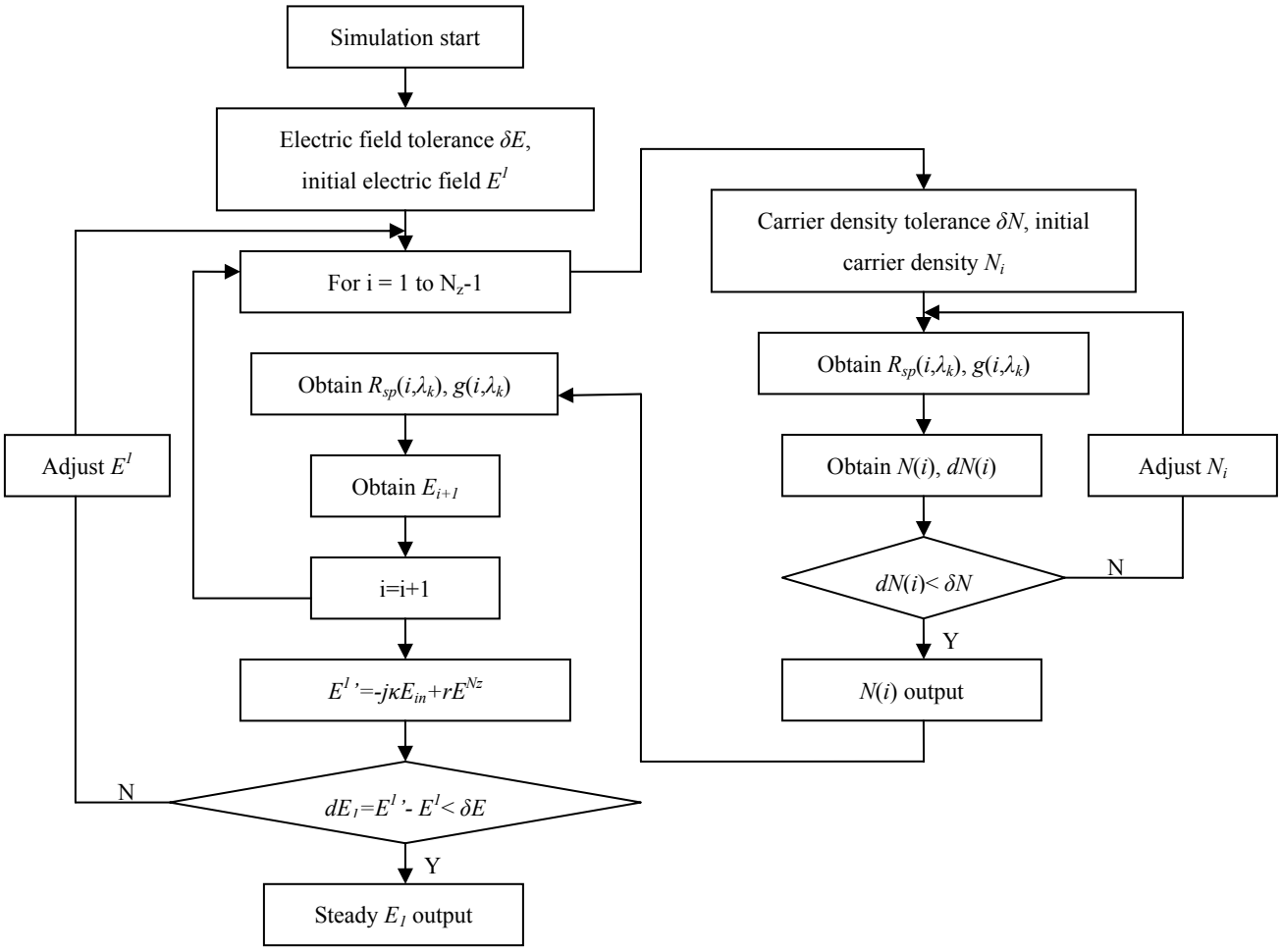

Fig. 2. Flowchart of the steady-state numerical algorithm

The steady-state numerical algorithm finds the steady electric field intensity in the active microring for given the injection current and power. The electric field intensity in subsection 1 is considered. Initially, we give an assumed electric field E^l in subsection 1. Based on carrier rate equation, the steady carrier density N_1 in subsection 1 under an electric field E^l can be determined associated with the material gain and the ASE noises. After that, since the light field

E^2 and steady carrier density N_2 can be calculated by E^1 and N_1. After Nz-1 times of iteration, the light field and carrier density distribution along the active microring can be calculated for the assumed electric field E^1 in subsection 1. The electric field mismatch dE can be calculated by

$$dE = E^{1'} - E^1 = \left(-j\kappa E_{in} + rE^{Nz}\right) - E^1 \tag{7}$$

All the iteration is implemented following the Muller iteration method. If the iterated dE below the electric field mismatch tolerance dE , then the steady state iteration is completed. Material parameters for the device simulation are given in Table 1.

Table. 1 Material parameters for the device simulation

Symbol	Parameter	Value
Effective radius	R_{eff}	20μm
Waveguide width	h	0.2μm
Waveguide height	d	1.0μm
Waveguide refractive index	n_1	3.35
Material loss	α_{in}	$1.5\times10^{4}\mathrm{m}^{-1}$
Optical field confinement factor	Γ	0.3
Linewidth enhancement factor	α_m	4
Coupling coefficient	κ	0.28
Spontaneous emission coupling coefficient	γ	0.0001
Linear nonradiative recombination coefficient	A	$3.5\times10^{8}\mathrm{s}^{-1}$
bimolecular nonradiative recombination coefficient	B	$5.6\times10^{-16}\ \mathrm{m}^{3}\mathrm{s}^{-1}$
Auger recombination coefficient	C	$3.0\times10^{-41}\ \mathrm{m}^{6}\mathrm{s}^{-1}$
Subsections	Nz	20

Figure 3 shows the calculated transmission spectrum of the active microring for different injected power with a bias current of 7.1mA, which is below the lasing threshold current of 9.9mA. We can see that the transmission spectrum red shifts as the injected power increases. This is for the reason that as the injected power increases, more carriers are consumed. According to the well-known K-K relationship, the effective index of the active region will increase, leading to a red shift.

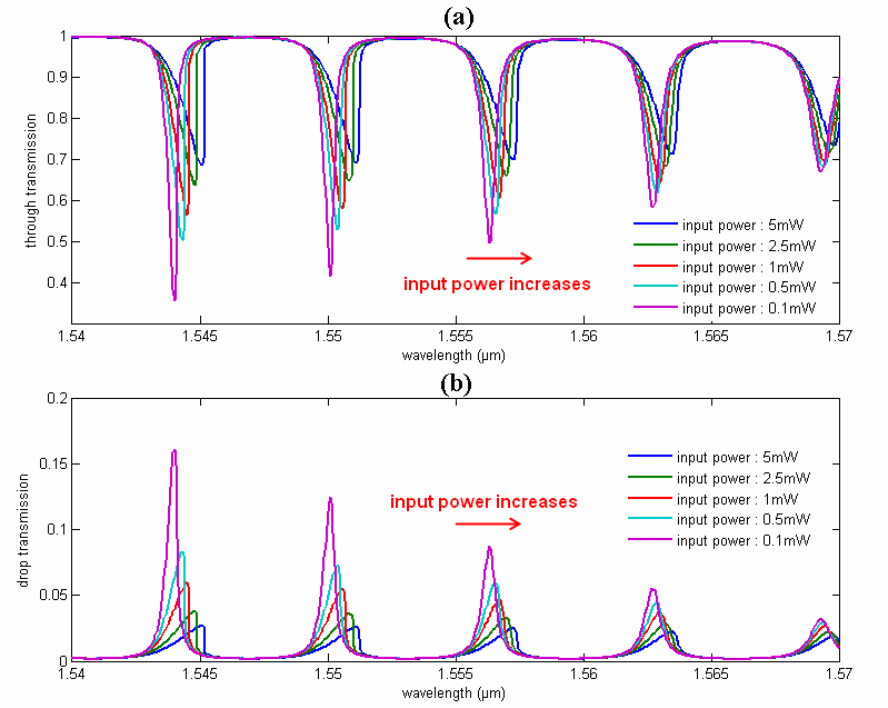

Fig. 3. Calculated transmission spectrum of the active microring for different injected power with a bias current of 7.1mA

Figure 4 shows the calculated transmission spectrum of the active microring for different bias current with an injected power of 1mW. The transmission spectrum blue-shifts as the bias current increases. This is because that as the bias current increases, more carriers are injected into the active region, leading to the effective index decreasing of the active region, hence the transmission spectrum will blue shift.

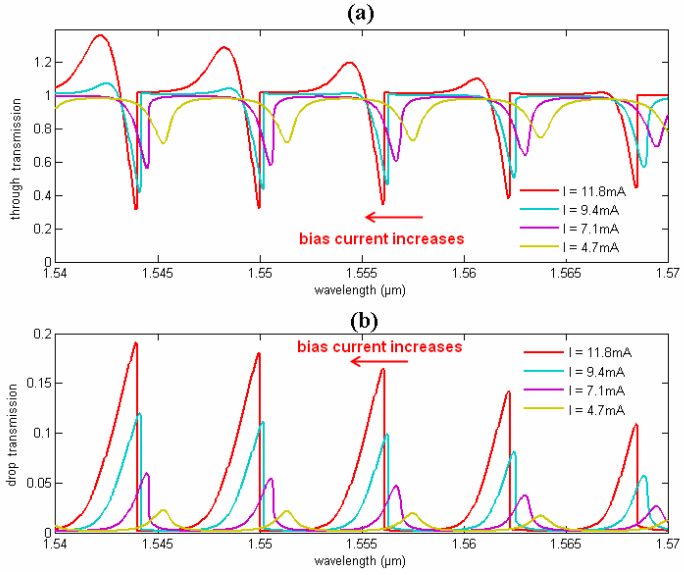

Fig. 4. Calculated transmission spectrum of the active microring for different bias current with an injected power of 1mW

3.2 Optical switching based on probe-pump method

Taking notice of the transmission spectrum of the active microring as shown in Fig.5, the spectrum slope of the right part is much steeper than the left part, which means that if the probe light is off-resonation initially, slightly red shift besides the right spectrum slope part, only little refractive index change will be need for the on-off switch to on-resonation. However, if the probe light is chosen to be on-resonation, much more refractive index change must be need for the on state switching to the off state.

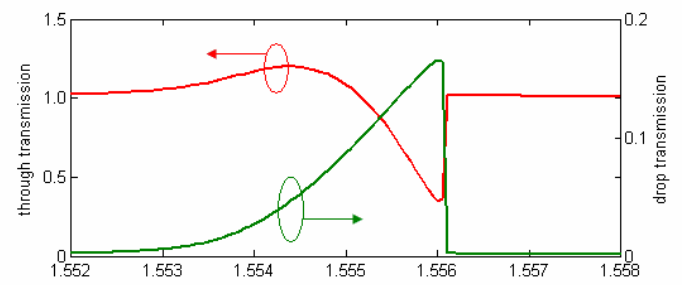

Fig. 6. Transmission spectrum of the active microring with the injected power of P_{probe}=1mW and bias current of I=9.4mA.

Figure 7 shows the on-off switching utilizing pump-probe method, with Injected probe power P_{probe}=1mW, bias current I=9.4mA, and pump light on resonation. As shown in Fig. 7(a), when the wavelength of the probe light is 1.5566μm, initially off resonation, only 0.8mW pump light is required for the off-on switching. However, if the probe light is 1.55626μm, initially on resonation, 5mW pump light must be required for the on-off switching. On the other hand, for the low bias current, the carrier life time is very long, resulting that more time is required for carrier recovery for the low power off-on switching.

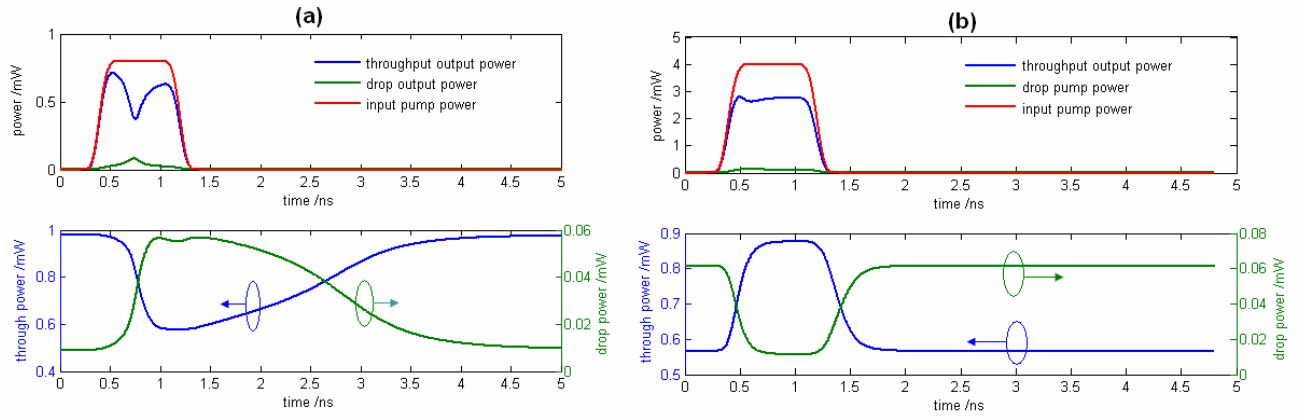

Fig. 7. On-off switching utilizing pump-probe method. (a) probe light initially off resonation. (b) probe light initially on resonation. Injected probe power P_{probe}=1mW, bias current I=9.4mA.

4. CONCLUSION

We have theoretically analyzed and numerically simulated the electrically pumped InGaAsP/InP active microring based on subsection model. The spectrum characteristics are numerically investigated, which shows an agreement with the previously reported results. The spectrum will shift under different pump current and injected light power. The

performances of an optical on/off switching utilizing pump-probe method based on InGaAsP/InP active microring are also investigated. The results show that if we choose pump light on resonation and probe light initially off resonation, only several hundred of microwatt power of pump light can realize the probe light on/off conversion. Such a potential will be applied in many other optical applications with ultra low power consumption. However, carrier lifetime will be the main factor restricting the recovery time.

ACKNOWLEDGEMENT

This research was sponsored by the National Natural Science Foundation of China (Grant No. 60577007), the National Basic Research Program of China (Grant No. 2006CB302805), and the Program for New Century Excellent Talents in University of Ministry of Education of China (Grant No. NCET-04-0715).

REFERENCES

1. M.T. Hill, M.T. Hill, S. Anantathanasarn, Y. Zhu, Y.S.A.O.Y.S. Oei, P.J.A.v.V.P.J. van Veldhoven, M.K.A.S.M.K. Smit and R.A.N.R. Notzel, "InAs–InP (1.55-um Region) Quantum-Dot Microring Lasers," IEEE Photon. Technol. Lett. 20(6), 446-448 (2008)
2. G.H. Yuan and S.Y. Yu, "Analysis of dynamic switching Behavior of bistable semiconductor ring lasers triggered by resonant optical pulse injection," IEEE J. Select. Top. Quantum Electron. 13(5), 1227-1234 (2007)
3. D. Alexandropoulos, H. Simos, M.J. Adams and D. Syvridis, "Optical bistability in active semiconductor microring structures," IEEE J. Select. Top. Quantum Electron. 14(3), 918-926 (2008)
4. M.T. Hill, H.J.S. Dorren, T. de Vries, X.J.M. Leijtens, J.H. den Besten, B. Smalbrugge, Y.S. Oei, H. Binsma, G.D. Khoe and M.K. Smit, "A fast low-power optical memory based on coupled micro-ring lasers," Nature 432(7014), 206-209 (2004)
5. S.C. Hagness, D. Rafizadeh, S.T. Ho and A. Taflove, "FDTD microcavity simulations: design and experimental realization of waveguide-coupled single-mode ring and whispering-gallery-mode disk resonators," IEEE J. Lightwave Technol. of 15(11), 2154 (1997)
6. E.B. Zhou, X.L. Zhang and D.X. Huang, "Analysis on dynamic characteristics of semiconductor optical amplifiers with certain facet reflection based on detailed wideband model," Opt. Express 15(14), 9096-9106 (2007)
7. J.J. Dong, S.N. Fu, X.L. Zhang, P. Shum, L.R. Zhang, J. Xu and D.X. Huang, "Single SOA based all-optical adder assisted by optical bandpass filter: Theoretical analysis and performance optimization," Opt. Commun 270(2), 238-246 (2007)
8. J.M. Mads L. Nielsen, Rei Suzuki, Jun Sakaguchi, Yoshiyasu Ueno, "Experimental and theoretical investigation of the impact of ultra-fast carrier dynamics on high-speed SOA-based all-optical switches," Opt. Express 14(1), 331-347 (2006)
9. J. Park, X. Li and W.P. Huang, "Comparative study of mixed frequency-time-domain models of semiconductor laser optical amplifiers," IEE P-Optoelectron. 152(3), 151-159 (2005)
10. J. Park and Y. Kawakami, "Time-domain models for the performance simulation of semiconductor optical amplifiers," Opt. Express 14(7), 2956-2968 (2006)